THE JOURNAL OF PHYSICAL CHEMISTRY C

Article

pubs.acs.org/JPCC

Role of Cerium Oxide in the Enhancement of Activity for the Oxygen Reduction Reaction at Pt−CeO_x Nanocomposite Electrocatalyst - An in Situ Electrochemical X-ray Absorption Fine Structure Study

Takuya Masuda,[†] Hitoshi Fukumitsu,[†,‡] Keisuke Fugane,[†,‡] Hirotaka Togasaki,[†,‡] Daiju Matsumura,[§] Kazuhisa Tamura,[§] Yasuo Nishihata,[§] Hideki Yoshikawa,[∥] Keisuke Kobayashi,[∥] Toshiyuki Mori,[†,‡] and Kohei Uosaki*[,†,‡,⊥]

[†]Global Research Center for Environment and Energy based on Nanomaterials Science (GREEN), National Institute for Materials Science (NIMS), Tsukuba, Ibaraki 305-0044, Japan

[‡]Division of Chemistry, Graduate School of Science, Hokkaido University, Sapporo, Hokkaido 060-0810, Japan

[§]Quantum Beam Science Directorate, Japan Atomic Energy Agency (JAEA), Sayo, Hyogo 679-5148, Japan

[∥]Synchrotron X-ray Station at SPring-8, National Institute for Materials Science (NIMS), Sayo, Hyogo 679-5148, Japan

[⊥]International Center for Materials Nanoarchitechtonics (WPI-MANA), National Institute for Materials Science (NIMS), Tsukuba, Ibaraki 305-0044, Japan

ABSTRACT: In situ electrochemical X-ray absorption fine structure (XAFS) measurements were performed at the Pt L_3 and Ce L_3 edges of the Pt−CeO_x/C catalyst, which was prepared by a combined process of precipitation and coimpregnation methods, as well as at the Pt L_3 edge of the conventional Pt/C catalyst in oxygen-saturated H_2SO_4 solution to clarify the role of CeO_x in the reduction of the overpotential for the oxygen reduction reaction (ORR) at the Pt−CeO_x nanocomposite compared with the conventional Pt/C catalyst. XAFS measurements clearly show that the enhancement of ORR activity is attributed to the inhibition of Pt oxide formation by the CeO_x layer, of which Ce^{3+} was oxidized to Ce^{4+} instead of Pt at the Pt oxide formation potential.

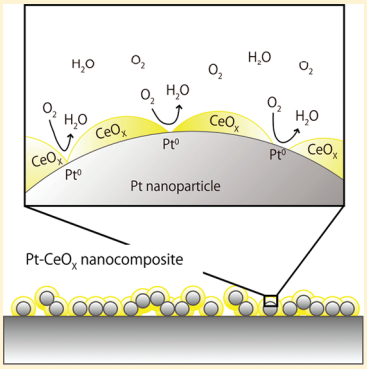

INTRODUCTION

Fuel cells, especially polymer electrolyte membrane (PEM) fuel cells, are expected to be one of the key devices to solve energy and environmental problems because of their very high theoretical efficiency and relatively low emission.[1] Many theoretical and experimental studies have been carried out toward its widespread use.[2,3] Platinum is the most-widely used electrocatalyst for both anode and cathode electrodes in the PEM fuel cell because of its excellent catalytic activity for various fuel cell reactions, such as the hydrogen oxidation reaction (HOR),[4] oxygen reduction reaction (ORR),[5] and methanol oxidation reaction (MOR).[6,7] However, potential loss at the cathode caused by relatively slow kinetics of the ORR is a critical issue to be solved for further improvement of the cell performance. Extensive research has been carried out to understand the ORR mechanism and reduce the potential losses.[5,8] One of the important approaches is to use cocatalysts in combination with platinum. A variety of transition metals have been used as cocatalysts, and several binary and ternary Pt−alloy systems have been proved to be effective for the enhancement of ORR activity.[9−14]

Cerium oxide (CeO_x) is known to be an excellent additive to promote various catalytic reactions,[15] especially for the elimination of toxic exhaust gases of automobiles by three-way catalysts,[16] due to its very unique oxygen storage capability. Recently, CeO_x has been also utilized as a cocatalyst with Pt catalyst for ORR in PEM fuel cells.[17−19] Although the effect of CeO_x as a promoter is considered to be due to its unique oxygen storage capability and substantial interaction between Pt and CeO_x, the detail of the role of CeO_x in the promotion of ORR is not well-understood.

X-ray absorption fine structure (XAFS) is a powerful technique to determine the local geometric and electronic structures of X-ray absorbing atoms[20] and has been used to monitor the potential-dependent local structure of the electrode under in situ electrochemical conditions,[21−27] including fuel cell reactions, but only very limited systematical studies are available to clarify the mechanism of catalytic reactions promoted by multicomponent catalysts, such as oxygen reduction based on simultaneous determination of the structures of all components.

Received: February 15, 2012
Revised: April 6, 2012
Published: April 25, 2012

dx.doi.org/10.1021/jp301509t | J. Phys. Chem. C 2012, 116, 10098−10102

In the present study, the promotion effect of CeO_x in the Pt−CeO_x/C catalyst for oxygen reduction is investigated by in situ XAFS measurements at the Pt L_3 and Ce L_3 edges of the Pt−CeO_x/C catalyst as well as at the Pt L_3 edge of the conventional Pt/C catalyst in oxygen-saturated H_2SO_4 solution.

EXPERIMENTAL SECTION

Ultrapure N_2 (99.99995%) and O_2 (99.99995%) were purchased from Taiyo Nissan. Ultrapure reagent grade H_2SO_4 and ultra-high-purity $(NH_4)_2CO_3$ from Wako Pure Chemicals, $H_2PtCl_6{\cdot}6H_2O$ (purity, 98.5%) from Kishida Chemicals, $Ce(NO_3)_3{\cdot}6H_2O$ (purity, >99.99%) from Kanto Chemicals, and carbon black (Vulcan XC-72R) from Cabot were used as received. Water was purified using a Milli-Q system (Yamato, WQ-500). A glassy carbon electrode, and Ag (99.99%) and Pt wires (99.99%) were purchased from Tokai Carbon and Nilaco, respectively.

Commercially available Pt/C (Johnson-Matthey) was used as received. Pt−CeO_x/C was synthesized by a combined process of precipitation and coimpregnation methods, as reported previously.[17,28,29] A 5 μL portion of an aqueous dispersion containing 20 wt % Pt/C or Pt−CeO_x/C was drop-cast on glassy carbon (Tokai Carbon) and then dried in an oven at 60 °C for 1 h. Prior to each experiment, the electrode surface was cleaned by an oxidation reduction cycle (ORC) between −0.2 and +1.3 V in 0.5 M H_2SO_4 solution saturated with nitrogen. Pt−CeO_x nanocomposites were characterized by X-ray diffraction (XRD), transmission electron microscopy (TEM), and X-ray photoelectron spectroscopy (XPS), as reported in the previous paper.[17] The electron diffraction pattern of the electrochemically pretreated sample showed a broad periodic ring, which is a common feature of amorphous-like materials, corresponding to the Bragg diffraction of Ce_2O_3.[17]

The electrochemical potential was controlled by an automatic polarization unit (Hokuto Denko, HSV-100). A Ag/AgCl electrode and a Pt wire were used as a reference and a counter electrode, respectively. Rotating disk electrode measurement was performed using a dynamic electrode controller (Hokuto Denko, HR201 and 202).

XAFS measurements at the Ce L_3 and Pt L_3 edges were carried out in fluorescence mode by using a silicon (111) double crystal monochromator and a 19-element pure-Ge solid-state detector (SSD, Canberra) at bending magnet beamline BL14B1 of SPring-8. A homemade spectroelectrochemical cell made of polychlorotrifluoroethylene (PCTFE) was used for the in situ XAFS measurements.[30] The cell was sealed with a 6.0 μm thick Mylar film (Chemplex), which serves as an X-ray window. The glassy carbon electrodes were pushed to the Mylar window, and thickness of the electrolyte solution layer between the electrode and window was ca. 30 μm so that X-ray scattering by the solution was avoided. Reference and counter electrodes were arranged in different compartments and shielded by a lead plate to avoid X-ray scattering by these components. The spectroelectrochemical cell was set on a κ-type six-circle diffractometer (Newport), and in situ XAFS measurements were carried out at various potentials in 0.5 M H_2SO_4 saturated with oxygen.

RESULTS AND DISCUSSION

Solid lines in Figure 1 show cyclic voltammograms (CVs) of Pt/C (red) and Pt−CeO_x/C (blue) electrodes measured in 0.5 M H_2SO_4 solution saturated with Ar. The CV of the Pt/C

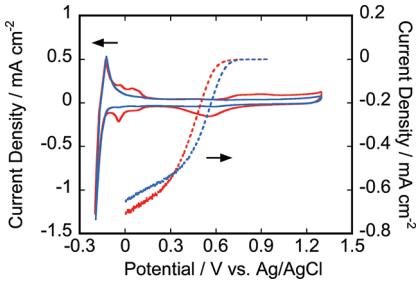

Figure 1. CVs (solid line) and LSVs (broken line) of the Pt/C (red line) and Pt−CeO_x/C (blue line) drop-cast glassy carbon electrodes measured in a 0.5 M H_2SO_4 solution saturated with Ar (CVs) and O_2 (LSVs) with a scan rate of 50 mV/s. LSVs in the O_2-saturated solution were obtained using a rotating disk electrode configuration at 2000 rpm.

electrode is almost identical to those of Pt polycrystalline and Pt/C electrodes reported previously.[31] Typical hydrogen adsorption/desorption and oxide formation/reduction waves and current due to the hydrogen evolution reaction (HER) were observed.

The CV of the Pt−CeO_x/C electrode is totally different from those of the Pt polycrystalline and the Pt/C electrodes. Hydrogen adsorption/desorption waves were absent, and oxide formation/reduction waves were significantly suppressed, showing the modulation of the electronic structure of Pt by the presence of CeO_x.

Broken lines in Figure 1 show linear sweep voltammograms (LSVs) of the Pt/C (red) and Pt−CeO_x/C (blue) electrodes measured in a 0.5 M H_2SO_4 solution saturated with O_2 in rotating disk electrode configuration at 2000 rpm with a scan rate of 50 mV/s. It is clear that ORR current at the Pt−CeO_x/C electrode started to flow at a more positive potential than that at the Pt/C electrode by 50−80 mV, showing the enhancement of the ORR rate by the addition of CeO_x to Pt. The onset potential of ORR at the Pt/C electrode coincides with the Pt oxide reduction potential observed in the Ar-saturated solution, suggesting that the Pt surface of the Pt/C was partially covered with Pt oxide near the onset of ORR. On the other hand, Pt oxide formation seemed to be inhibited at the Pt−CeO_x/C electrode. Thus, it appears that the enhancement of ORR at the Pt−CeO_x/C is attributed to the suppression of Pt oxide formation.

To understand the role of CeO_x on the enhancement of catalytic activity more quantitatively, XAFS measurements were carried out. Figures 2 and 3 show X-ray absorption near-edge structure (XANES) spectra of the Pt−CeO_x/C electrode at the

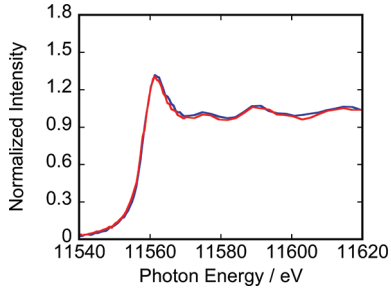

Figure 2. Normalized XANES spectra at the Pt L_3 edge for the Pt−CeO_x/C electrode before (red line) and after (blue line) the pretreatment.

dx.doi.org/10.1021/jp301509t | J. Phys. Chem. C 2012, 116, 10098−10102

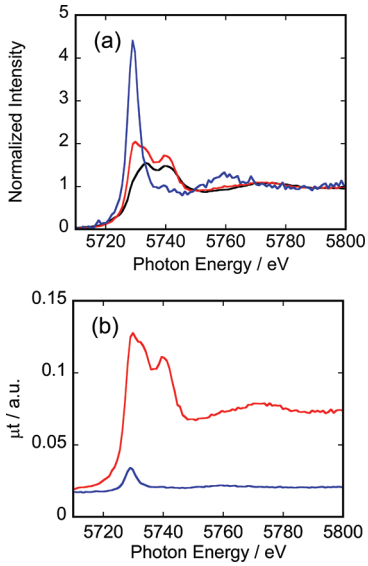

Figure 3. (a) Normalized XANES spectra at the Ce L_3 edge for pure CeO_2 powder in air (black line), and the Pt−CeO_x/C electrode before (red line) and after (blue line) immersing in 0.5 M H_2SO_4 solution for 30 min. (b) Absolute XANES spectra at the Ce L_3 edge for the Pt−CeO_x/C electrode before (red line) and after (blue line) immersing in 0.5 M H_2SO_4 solution for 30 min.

Pt L_3 edge before and after the pretreatment, that is, oxidation/reduction cycles (ORCs) in N_2-saturated 0.5 M H_2SO_4 solution for cleaning and the Ce L_3 edge after each treatment step, respectively. A peak was observed around 11 560 eV in Figure 2 and should correspond to Pt in the metal state as the white line (WL) intensity is not so large.[32] No change was observed before and after the pretreatment, showing that the amount and oxidation state of Pt were not affected by the pretreatment.

On the other hand, XANES spectra at the Ce L_3 edge (Figure 3) show the significant effect of the treatments on the amount and the oxidation state of Ce. While typical doublet peaks corresponding to Ce^{4+} were observed at 5733 and 5740 eV for pure CeO_2 powder (Figure 3a),[33] confirming that the CeO_2 is the dominant species, not only the doublet peaks but also a new small peak around 5729 eV, which corresponds to Ce^{3+}, were observed when Pt was incorporated, showing the formation of Ce^{3+} species as a result of the incorporation of Pt.[33] After the Pt−CeO_x/C was immersed in a 0.5 M H_2SO_4 solution for ORC, absorbance decreased to ~6% (Figure 3b), implying the dissolution of CeO_x. The normalized XANES spectrum shows the preferential dissolution of Ce^{4+} species as only the Ce^{3+} peak was observed. The loss of CeO_2 during the pretreatment was confirmed by XPS.[17] On the basis of these observations, it is concluded that CeO_2 was dissolved in sulfuric acid solution and the Pt−CeO_x nanocomposite was formed during the pretreatment, as schematically illustrated in Figure 4. The TEM image of the Pt−CeO_x nanocomposite presented in a previous report showed the formation of the Pt/CeO_x interface.[17] Despite the formation of the CeO_x/Pt interface, no change was observed in the XANES spectra at the Pt L_3 edge for the Pt−CeO_x/C (Figure 2), probably due to the relatively small ratio of surface to bulk atoms of Pt particles.

After the pretreatment, XAFS spectra at the Pt L_3 edge were obtained for the Pt/C and Pt−CeO_x/C electrodes at various potentials in a 0.5 M H_2SO_4 solution saturated with O_2. Figure 5 shows potential dependencies of the current (expansion of

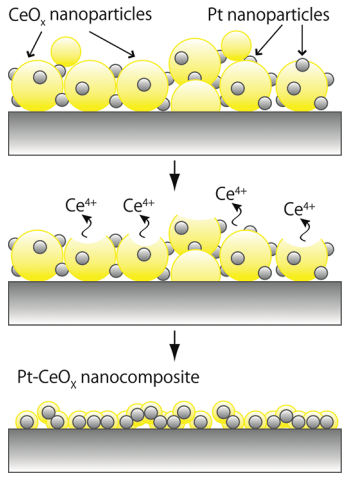

Figure 4. Schematic illustration of structural change of the Pt−CeO_x/C catalyst during the pretreatment.

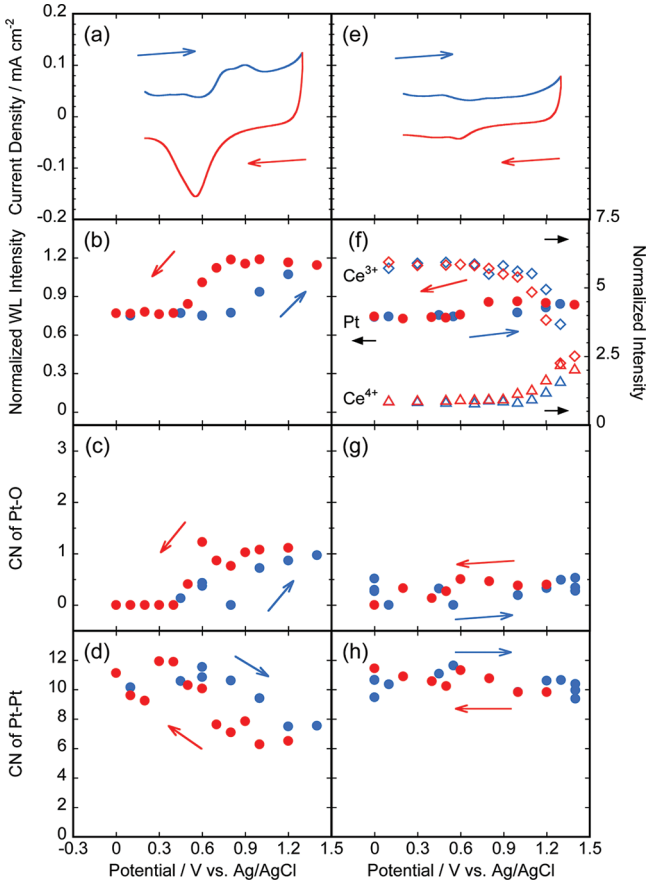

Figure 5. (a, e) Current, (b, f) normalized white line (WL) intensities, and coordination number (CN) of (c, g) O and (d, h) Pt around Pt of the (a−d) Pt/C and (e−h) Pt−CeO_x/C electrodes as a function of potential in the positive- (blue) and negative (red)-going scans.

the results presented in Figure 1), normalized WL intensities, and coordination numbers (CNs) of O and Pt around Pt of the Pt/C and Pt−CeO_x/C electrodes, which were obtained by curve fitting of the extended X-ray absorption fine structure (EXAFS).

When the potential at the Pt/C electrode was made positive, these three parameters did not change up to 0.8 V, but then the WL intensity increased and CNs of O and Pt around Pt

dx.doi.org/10.1021/jp301509t | J. Phys. Chem. C 2012, 116, 10098−10102

increased and decreased, respectively, as the potential became more positive (Figure 5b–d). Since the WL intensity of the Pt L_3 absorption edge reflects d-band vacancy,[32] the increase in the WL intensity suggests the formation of Pt oxide, confirming the results of electrochemical measurements, which showed the flow of anodic current corresponding to Pt oxide formation from 0.6 V (Figures 1 and 5a). Potential dependencies of CNs confirm Pt oxide formation because, if Pt oxide is formed, oxygenated species are adsorbed on the Pt surface and oxygen is penetrated into the Pt lattice, leading to the increase and decrease of CNs of O and Pt, respectively, around Pt, as experimentally observed. In the negative-going potential scan, the WL intensity of Pt L_3 absorption edge (Figure 5b) as well as CNs of O (Figure 5c) and Pt (Figure 5d) returned to the original values at around 0.6 V where cathodic current peak due to the reduction of oxide was observed (Figure 5a), showing the reversible formation and reduction of Pt oxide.

In contrast to the above mentioned results obtained at the Pt/C electrode, potential dependent changes of WL intensity of Pt L_3 absorption edge (Figure 5f) and CNs of O (Figure 5g) and Pt (Figure 5h) around Pt at the Pt–CeO_x/C electrode were very small, showing the suppression of Pt oxide formation at the Pt–CeO_x/C electrode. This is in agreement with the result shown in Figures 1 and 5e that only a very small current due to oxide formation/reduction was observed at the Pt–CeO_x/C. One may consider that this difference was caused by the difference in the particle size because only surface Pt atoms are subjected to oxidization/reduction, but all Pt atoms within the particle contribute to the XAFS spectrum. Thus, when Pt oxide is formed on the surface of larger particles, at which the fraction of surface atoms to bulk atoms is smaller, smaller changes in the above parameters are expected. According to TEM observations, however, the size of the Pt nanoparticles of the Pt–CeO_x/C was almost the same as that of the Pt/C used in the present study, that is, 3–5 nm,[17] and therefore, one can conclude that the XAFS results showed that the oxidation of the Pt surface at the Pt–CeO_x/C was indeed suppressed. The inhibition of Pt oxide formation by the presence of CeO_x should be one of the primary reasons for the enhancement of the ORR rate at the Pt–CeO_x/C electrode because the oxide-covered Pt surface is known to exhibit a lower catalytic activity for ORR than the bare Pt surface.[34−37]

To examine the role of CeO_x in inhibiting the Pt oxide formation, in situ XAFS measurement at the Ce L_3 edge for the Pt–CeO_x/C was also carried out at various potentials in 0.5 M H_2SO_4 solution saturated with O_2 after the pretreatment. Potential-dependent WL intensities at 5729 and 5740 eV corresponding to the Ce^{3+} and Ce^{4+}, respectively, are shown in Figure 5f together with that of Pt. The EXAFS oscillation was too weak for curve fitting to determine the CN because of a very small quantity of CeO_x. In the relatively negative potential region between 0.2 and 0.9 V, a peak at 5729 eV corresponding to Ce^{3+} species was dominant, and the intensity of this peak was almost constant within this potential region. When the potential became more positive than 0.9 V, at which Pt oxide formation started at the Pt/C electrode without CeO_x, intensities of the Ce^{3+} and Ce^{4+} peaks decreased and increased, respectively, showing the oxidation of Ce^{3+} to Ce^{4+}. In the reverse scan, Ce^{4+} was reduced to Ce^{3+} with a very small hysteresis. It looks like Pt oxide formation is suppressed by the sacrificial oxidation of Ce^{3+} to Ce^{4+}, and as a result, the ORR rate is enhanced because ORR takes place at the metallic Pt^0 site, as shown in Figure 6, where the ORR rate is much faster

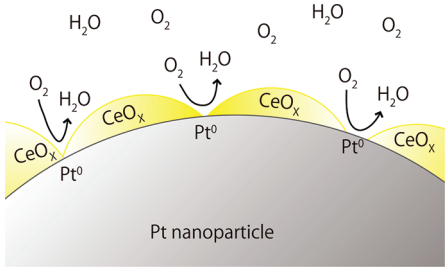

Figure 6. Schematic illustration of ORR at the Pt–CeO_x nanocomposite.

than that at Pt oxide. The redox behavior of Ce^{3+}/Ce^{4+} of the Pt–CeO_x/C electrode is significantly different from the one previously reported for CeO_x on a graphite electrode without Pt[38] at which the anodic current corresponding to the oxidation of Ce^{3+} to Ce^{4+} flowed from 1.1 V,[38] whereas the oxidation of Ce^{3+} to Ce^{4+} started at around 0.9 V in the present system (Figure 5f). Thus, while Pt became more difficult to be oxidized, the oxidation of Ce^{3+} to Ce^{4+} became easier at the Pt–CeO_x system. These behaviors can be explained by the partial electron transfer from Ce^{3+} to Pt.

■ CONCLUSIONS

The role of CeO_x in the enhancement of the ORR rate at the Pt/C catalyst was clarified by in situ XAFS measurements at the Pt L_3 and Ce L_3 edges of the Pt–CeO_x/C catalyst as well as at the Pt L_3 edge of the conventional Pt/C catalyst in oxygen-saturated H_2SO_4 solution. It was shown that Pt oxide formation was suppressed by the presence of CeO_x as Ce^{3+} was oxidized to Ce^{4+} instead of Pt at the Pt oxide formation potential. The inhibition of Pt oxide formation is considered to be the primary factor for enhancement of the ORR rate because ORR activity of the Pt oxide surface is much lower than that at the bare Pt surface.

■ AUTHOR INFORMATION

Corresponding Author

*E-mail: uosaki.kohei@nims.go.jp. Tel: +81-29-860-4301. Fax: +81-29-851-3362.

Notes

The authors declare no competing financial interest.

■ ACKNOWLEDGMENTS

The present work was partially supported by the World Premier International Research Center (WPI) Initiative on Materials Nanoarchitectonics and MEXT Program for Development of Environmental Technology using Nanotechnology from Ministry of Education, Culture, Sports, Science and Technology, Japan. Synchrotron radiation experiments were performed as projects approved by the Japan Synchrotron Radiation Research Institute (JASRI) (proposal nos. 2006A1615, 2006B3611, and 2007A3629) and the Photon Factory Program Advisory Committee (PAC Nos. 2007G079 and 2009G014).

■ REFERENCES

(1) Kordesch, K. V.; Simader, G. R. *Chem. Rev.* **1995**, *95*, 191–207.
(2) Wang, C. Y. *Chem. Rev.* **2004**, *104*, 4727–4765.
(3) Borup, R.; Meyers, J.; Pivovar, B.; Kim, Y. S.; Mukundan, R.; Garland, N.; Myers, D.; Wilson, M.; Garzon, F.; Wood, D.; Zelenay, P.; More, K.; Stroh, K.; Zawodzinski, T.; Boncella, J.; McGrath, J. E.;

Inaba, M.; Miyatake, K.; Hori, M.; Ota, K.; Ogumi, Z.; Miyata, S.; Nishikata, A.; Siroma, Z.; Uchimoto, Y.; Yasuda, K.; Kimijima, K. I.; Iwashita, N. *Chem. Rev.* **2007**, *107*, 3904−3951.
(4) Gasteiger, H. A.; Markovic, N. M.; Ross, P. N. *J. Phys. Chem.* **1995**, *99*, 8290−8301.
(5) Markovic, N. M.; Schmidt, T. J.; Stamenkovic, V.; Ross, P. N. *Fuel Cells* **2001**, *1*, 105−116.
(6) Burstein, G. T.; Barnett, C. J.; Kucernak, A. R.; Williams, K. R. *Catal. Today* **1997**, *38*, 425−437.
(7) Baxter, S. F.; Battaglia, V. S.; White, R. E. *J. Electrochem. Soc.* **1999**, *146*, 437−447.
(8) Strmcnik, D.; Escudero-Escribano, M.; Kodama, K.; Stamenkovic, V. R.; Cuesta, A.; Markovic, N. M. *Nat. Chem* **2010**, *2*, 880−885.
(9) Mukerjee, S.; Srinivasan, S. *J. Electroanal. Chem.* **1993**, *357*, 201−224.
(10) Tamizhmani, G.; Capuano, G. A. *J. Electrochem. Soc.* **1994**, *141*, 968−975.
(11) Toda, T.; Igarashi, H.; Uchida, H.; Watanabe, M. *J. Electrochem. Soc.* **1999**, *146*, 3750−3756.
(12) Paulus, U. A.; Wokaun, A.; Scherer, G. G.; Schmidt, T. J.; Stamenkovic, V.; Radmilovic, V.; Markovic, N. M.; Ross, P. N. *J. Phys. Chem. B* **2002**, *106*, 4181−4191.
(13) Stamenkovic, V. R.; Mun, B. S.; Arenz, M.; Mayrhofer, K. J. J.; Lucas, C. A.; Wang, G. F.; Ross, P. N.; Markovic, N. M. *Nat. Mater.* **2007**, *6*, 241−247.
(14) Stamenkovic, V. R.; Fowler, B.; Mun, B. S.; Wang, G. F.; Ross, P. N.; Lucas, C. A.; Markovic, N. M. *Science* **2007**, *315*, 493−497.
(15) Summers, J. C.; Ausen, S. A. *J. Catal.* **1979**, *58*, 131−143.
(16) Harrison, B.; Diwell, A. F.; Hallet, C. *Platinum Met. Rev.* **1988**, *32*, 73−83.
(17) Fugane, K.; Mori, T.; Ou, D. R.; Suzuki, A.; Yoshikawa, H.; Masuda, T.; Uosaki, K.; Yamashita, Y.; Ueda, S.; Kobayashi, K.; Okazaki, N.; Matolinova, I.; Matolin, V. *Electrochim. Acta* **2011**, *56*, 3874−3883.
(18) Yu, H. B.; Kim, J. H.; Lee, H. I.; Scibioh, M. A.; Lee, J.; Han, J.; Yoon, S. P.; Ha, H. Y. *J. Power Sources* **2005**, *140*, 59−65.
(19) Lim, D. H.; Lee, W. D.; Choi, D. H.; Lee, H. I. *Appl. Catal., B* **2010**, *94*, 85−96.
(20) Iwasawa, Y. *X-ray Absorption Fine Structure for Catalyst and Surfaces*; World Scientific: Singapore, 1996.
(21) Mukerjee, S.; Srinivasan, S.; Soriaga, M. P.; Mcbreen, J. *J. Electrochem. Soc.* **1995**, *142*, 1409−1422.
(22) Mukerjee, S.; McBreen, J. *J. Electroanal. Chem.* **1998**, *448*, 163−171.
(23) Yoshitake, H.; Mochizuki, T.; Yamazaki, O.; Ota, K. *J. Electroanal. Chem.* **1993**, *361*, 229−237.
(24) Yoshitake, H.; Yamazaki, O.; Ota, K. *J. Electrochem. Soc.* **1994**, *141*, 2516−2522.
(25) Tada, M.; Murata, S.; Asakoka, T.; Hiroshima, K.; Okumura, K.; Tanida, H.; Uruga, T.; Nakanishi, H.; Matsumoto, S.; Inada, Y.; Nomura, M.; Iwasawa, Y. *Angew. Chem., Int. Ed.* **2007**, *46*, 4310−4315.
(26) Tamura, K.; Oyanagi, H.; Kondo, T.; Koinuma, M.; Uosaki, K. *J. Phys. Chem. B* **2000**, *104*, 9017−9024.
(27) Masuda, T.; Fukumitsu, H.; Takakusagi, S.; Chun, W. J.; Kondo, T.; Asakura, K.; Uosaki, K. *Adv. Mater.* **2012**, *24*, 268.
(28) Takahashi, M.; Mori, T.; Vinu, A.; Kobayashi, H.; Drennan, J.; Ou, D. R. *J. Mater. Res.* **2006**, *21*, 2314−2322.
(29) Takahashi, M.; Mori, T.; Vinu, A.; Ou, D. R.; Kobayashi, H.; Drennan, J. *Adv. Appl. Ceram.* **2008**, *107*, 57−63.
(30) Kondo, T.; Tamura, K.; Takahasi, M.; Mizuki, J.; Uosaki, K. *Electrochim. Acta* **2002**, *47*, 3075−3080.
(31) Perez, J.; Gonzalez, E. R.; Ticianelli, E. A. *Electrochim. Acta* **1998**, *44*, 1329−1339.
(32) Russell, A. E.; Rose, A. *Chem. Rev.* **2004**, *104*, 4613−4635.
(33) Zhang, J.; Ju, X.; Wu, Z. Y.; Liu, T.; Hu, T. D.; Xie, Y. N.; Zhang, Z. L. *Chem. Mater.* **2001**, *13*, 4192−4197.
(34) Damjanovic, A.; Hudson, P. G. *J. Electrochem. Soc.* **1988**, *135*, 2269−2273.
(35) Damjanovic, A. *J. Electrochem. Soc.* **1991**, *138*, 2315−2320.
(36) Markovic, N. M.; Gasteiger, H. A.; Grgur, B. N.; Ross, P. N. *J. Electroanal. Chem.* **1999**, *467*, 157−163.
(37) Markovic, N. M.; Ross, P. N. Electrocatalysis at Well-Defined Surfaces: Kinetics of Oxygen Reduction and Hydrogen Oxidation/Evolution on Pt(*hkl*) Electrodes. In *Interfacial Electrochemistry: Theory, Experiments and Applications*; Wieckowski, A., Ed.; Marcal Dekker Inc.: New York, 1999; p 821.
(38) Sharma, S.; Hegde, M. S. *J. Chem. Phys.* **2009**, *130*, 114706.